

Dirac gaugino as leptophilic dark matter

Eung Jin Chun and Jong-Chul Park

Korea Institute for Advanced Study, Heogiro 87, Dongdaemun-gu, Seoul 130-722, Korea

Emails: ejchun@kias.re.kr, jcpark@kias.re.kr

Stefano Scopel

*Department of Physics and Astronomy, Seoul National University
Gwanak-ro 599, Gwanak-gu, Seoul 151-742, Korea*

Email: scopel@phya.snu.ac.kr

ABSTRACT: We investigate the leptophilic properties of Dirac gauginos in an R-symmetric N=2 supersymmetric model with extended gauge and Higgs sectors. The annihilation of Dirac gauginos to leptons requires no chirality flip in the final states so that it is not suppressed as in the Majorana case. This implies that it can be sizable enough to explain the positron excess observed by the PAMELA experiment with moderate or no boost factors. When squark masses are heavy, the annihilation of Dirac gauginos to hadrons is controlled by their Higgsino fraction and is driven by the hZ and W^+W^- final states. Moreover, at variance with the Majorana case, Dirac gauginos with a non-vanishing Higgsino fraction can also have a vector coupling with the Z gauge boson leading to a sizable spin-independent scattering cross section off nuclei. Saturating the current antiproton limit, we show that Dirac gauginos can leave a signal in direct detection experiments at the level of the sensitivity of dark matter searches at present and in the near future.

Contents

1. Introduction	1
2. The R–symmetric gauge/Higgs sector and Dirac bino couplings	3
3. Indirect and direct signals of Dirac neutralino DM	7
3.1 Annihilations to $\bar{l}l$ and hZ	7
3.2 Annihilations through Z	8
3.3 Direct detection through Z and h exchange	9
4. Analysis	11
4.1 Constraints on leptophilic dark matter	11
4.2 The Dirac bino as a leptophilic DM candidate	13
4.3 The case of a Dirac neutralino of general composition	16
5. Conclusions	19

1. Introduction

N=1 supersymmetry broken around the weak scale would be the prime new physics candidate to be searched at the LHC. It provides not only an appealing explanation for the origin of the electroweak symmetry breaking but also a natural dark matter (DM) particle of the Universe. While N=1 supersymmetry is enforced by the chiral structure of matter fields in the Standard Model, the gauge sector may be extended to have N=2 supersymmetry in which gauginos can be Dirac particles [1, 2, 3, 4, 5, 6, 7, 8, 9] (for a review of N=2 supersymmetry, see [10]). Determining the Majorana/Dirac nature of gauginos will be an interesting task for future experiments looking for supersymmetric CP and flavor violation [11, 12], collider signatures [13, 14], and dark matter properties [15, 16, 17, 18].

There are some important distinctions between Majorana and Dirac gauginos. First, the annihilation of a Dirac gaugino pair into a fermion–antifermion pair, $\chi\bar{\chi} \rightarrow f\bar{f}$, has a non-vanishing s –wave contribution even in the limit of vanishing fermion masses, and thus the leptonic final states are not suppressed. This implies that a Dirac gaugino can provide a viable DM explanation for the abundance of energetic electrons and positrons recently observed in cosmic rays [19, 20, 21, 22, 23, 24, 25]. Second, Dirac gauginos can have a vector coupling with the Z gauge boson, $\bar{\chi}\gamma_{\mu}\chi Z^{\mu}$,

leading to sizable spin-independent scattering off nuclei. As a consequence, the Higgsino component in the DM gets constrained by the direct detection data [26] and also by the non-observation of antiproton excesses in PAMELA [27] as will be discussed in detail in the following.

In order to ensure such Dirac nature of DM, Majorana mass terms, which provide the mass splitting between the Dirac components, have to be highly suppressed. Otherwise, the heavier component of the two quasi-degenerate Majorana gauginos will decay to the lighter one, and the galactic DM will consist of a pure Majorana gaugino. If one assumes the N=2 structure in the Higgs sector, i.e. that the two Higgses H_u and H_d form an N=2 hypermultiplet [7, 8], the Dirac structure imposed at the tree level is spoiled by a large amount due to radiative corrections with Higgs-Higgsino and fermion-sfermion in the loop. A way to enforce an (almost) pure Dirac property for gauginos is then to assume a continuous R symmetry which forbids the usual μ term for the Higgs bilinear coupling $H_u H_d$ and the soft breaking trilinear A term [12].

In this paper, we will work out a framework for R-symmetric Dirac gauginos, which are introduced by extending the gauge/Higgs sector of a supersymmetric model. We assume the Dirac bino as the main component of the lightest supersymmetric particle. The annihilation of two Dirac binos into a lepton-antilepton pair usually dominates over the annihilation into a quark-antiquark pair, as sleptons are typically much lighter than squarks. As we will see, the annihilation to a CP even final or intermediate state turns out to be velocity-suppressed, which is a property that is also true in the usual Majorana gaugino case. Then, the Dirac bino annihilation to the two W bosons (W^+W^-) and that to a CP even Higgs boson and a Z boson (hZ), both controlled by the Higgsino component in the DM particle, turn out to be the next important sources of the cosmic antiproton flux. Quantifying the suppression factor for the Higgsino component, one can make a prediction for the direct detection rate.

In Section 2, an R-symmetric N=2 extension of the Minimal Supersymmetric Standard Model is introduced to enforce an almost pure Dirac gaugino structure. Based on this framework, we derive interaction vertices for the Dirac bino, which is assumed to be the dark matter, and then provide a qualitative analysis for its indirect and direct detection properties in Section 3. A numerical analysis is performed in Section 4 to obtain various fits and constraints of the leptophilic Dirac bino dark matter from the current indirect and direct detection data. We give our conclusions in Section 5.

2. The R–symmetric gauge/Higgs sector and Dirac bino couplings

Let us first note that a small Majorana mass term, breaking the Dirac structure, will produce quasi-degenerate two Majorana gauginos, the heavier of which will then decay to the lighter one. Assuming a tiny splitting δm_M in the Dirac bino components, one expects to have one–loop diagrams generating the magnetic moment operator:

$$\frac{\alpha'}{4\pi} \frac{m_{\tilde{B}}}{\tilde{m}^2} \tilde{B}_1 \Sigma_{\mu\nu} \tilde{B}_2 F^{\mu\nu}, \quad (2.1)$$

between two almost degenerate Majorana components ($m_{\tilde{B}_2} - m_{\tilde{B}_1} = \delta m_M$) where $m_{\tilde{B}} \approx m_{\tilde{B}_{1,2}}$ is the almost degenerate bino mass and \tilde{m} is a sfermion mass. The decay rate for the process $\tilde{B}_2 \rightarrow \tilde{B}_1 \gamma$ is

$$\Gamma \approx \frac{\alpha}{4\pi} \left(\frac{\alpha'}{4\pi} \frac{m_{\tilde{B}}^2}{\tilde{m}^2} \right)^2 \delta m_M. \quad (2.2)$$

In order to maintain the Dirac gaugino structure for the present DM, we require that its lifetime is larger than the age of the Universe. This gives us

$$\delta m_M \lesssim 10^{-33} \text{ GeV}, \quad (2.3)$$

for $m_{\tilde{B}} \sim \tilde{m}$. Thus, the Majorana gaugino mass term has to be suppressed below the order of $\delta m_M \ll m_{3/2}^3/M_P^2$, where $m_{3/2}$ is the gravitino mass ~ 1 TeV. In N=1 supergravity, a nonzero value of the superpotential w_0 is required to tune the cosmological constant. As w_0 breaks an R symmetry, it can usually generate Majorana gaugino masses of the order of $m_{3/2} \sim w_0$. In fact, avoiding such a leading contribution to gaugino masses and A or B soft supersymmetry breaking terms has been discussed in the context of split supersymmetry [28]. Furthermore, a loop contribution from anomaly mediation was also shown to be further suppressed [28, 29]. Concerning the anomaly mediation contribution, it is interesting to remark that, saturating the lower bound, one finds $\delta m_M \sim (g^2/16\pi^2)(1/16\pi^2)(m_{3/2}^3/M_P^2)$ [28] which can be compatible with the condition (2.3).

An almost R–symmetric supersymmetry breaking can be realized in the following way. Let us introduce an extended gauge–Higgs sector [12]:

$$W' = \mu_1 H_d R_u + \mu_2 R_d H_u - \sqrt{2} g_a (\xi_1 H_d T^a R_u + \xi_2 H_u T^a R_d) \Phi^a, \quad (2.4)$$

where $\Phi^a = (\phi^a, \psi^a)$ is the N=2 counterpart of the gauge superfield W_α^a . In our phenomenological approach, the N=2 structure is supposed to be broken in an appropriate way leading to an effective N=1 superpotential, as discussed below. For instance, $\xi_{1,2}$ in Eq. (2.4) are arbitrary parameters breaking the N=2 relation. Note

that the usual Higgs superfields $H_{d,u}$ cannot form an N=2 hypermultiplet as the corresponding μ and B terms, breaking an R symmetry, will generate a large Majorana mass $m_{1/2} \propto (\alpha/4\pi)\mu B$ at one-loop. A similar one-loop contribution arises also from the presence of left-right mixing sfermion masses, depending on the μ or A term. Thus, we are forced to extend the Higgs sector to avoid the usual μ and B terms and we will consider a situation in which the N=2 structure is not respected in the extended Higgs sector. Now let us introduce a supersymmetry breaking field X and two R symmetries, denoted by \mathcal{R} and \mathcal{J} , which are broken by two order parameters x_0 and w_0 . The R charge assignment is given by

$$\begin{array}{c|cccccc} & W_\alpha^a & \Phi^a & H_{d,u} & R_{u,d} & X & x_0 & w_0 \\ \hline \mathcal{R} & 1 & 2 & 0 & 0 & 0 & 2 & 2 \\ \mathcal{J} & 1 & 0 & -1 & 3 & 2 & 0 & 2 \end{array} . \quad (2.5)$$

Note that the two R symmetries are not compatible with the N=2 structure [10] as different \mathcal{J} charges are assigned to $H_{d,u}$ and $R_{u,d}$ and thus they are not considered to come from the same hypermultiplets. The superpotential of the supersymmetry breaking sector can be written as

$$W = w_0 + x_0 X , \quad (2.6)$$

which gives $\langle X \rangle = \theta^2 F_X$, where $F_X = x_0 \sim m_{3/2} \sim w_0$ is assumed. Now one can see that the Dirac gaugino mass and the extended μ terms can come from the following F or D terms:

$$XW_\alpha^a Q_\alpha \Phi^a|_F, \quad HR\Phi|_F \text{ or } HRX^\dagger|_D , \quad (2.7)$$

where Q_α is the supersymmetric covariant derivative. The last two terms in the above equation reproduce the superpotential (2.4) and the first term gives the Dirac gaugino mass term: $\mathcal{L}_{soft} = M_a \psi^a \tilde{W}^a$. In the following, we will concentrate on the Dirac gauginos in the electroweak sector. The Dirac bino (wino) mass is denoted by M_1 (M_2). The Majorana gaugino mass (and similarly the A term) gets a contribution from

$$W_\alpha^a W_\alpha^a W_0^\dagger X X^\dagger|_D . \quad (2.8)$$

This gives the (Majorana) soft term $\mathcal{L}_{soft} = \delta m_M \tilde{W}^a \tilde{W}^a$ with $\delta m_M \sim m_{3/2}^3/M_P^2$ which can be compatible with the bound (2.3) assuming a small coefficient of the order of 10^{-4} for $m_{3/2} \sim 300$ GeV. Thus, we can safely neglect the Majorana mass terms in our discussion.

Such a framework allows us to have highly suppressed Majorana mass terms and

results in the following R-symmetric gaugino-Higgsino mass matrix:

$$\mathcal{M} = \begin{bmatrix} 0 & M_1 & 0 & -\xi_1 m_Z s_W c_\beta & 0 & \xi_2 m_Z s_W s_\beta \\ M_1 & 0 & -m_Z s_W c_\beta & 0 & m_Z s_W s_\beta & 0 \\ 0 & -m_Z s_W c_\beta & 0 & \mu_1 & 0 & 0 \\ -\xi_1 m_Z s_W c_\beta & 0 & \mu_1 & 0 & 0 & 0 \\ 0 & m_Z s_W s_\beta & 0 & 0 & 0 & \mu_2 \\ \xi_2 m_Z s_W s_\beta & 0 & 0 & 0 & \mu_2 & 0 \end{bmatrix} \quad (2.9)$$

in the basis of $(\psi^0, \tilde{B}, \tilde{H}_d, \tilde{R}_u, \tilde{H}_u, \tilde{R}_d)$. Note that, in order to make a transparent discussion of the Dirac gaugino properties, we reduced the number of free parameters by decoupling the wino component which can be justified in the limit of heavy wino mass: $M_2 \gg M_1, |\mu_i|$.

The Dirac gaugino mass matrix (2.9) can be diagonalized by 6 angles which can be parameterized as

$$\mathcal{N} = \begin{bmatrix} c_1 & 0 & s_1 & 0 & 0 & 0 \\ 0 & c_4 & 0 & s_4 & 0 & 0 \\ -s_1 & 0 & c_1 & 0 & 0 & 0 \\ 0 & -s_4 & 0 & c_4 & 0 & 0 \\ 0 & 0 & 0 & 0 & 1 & 0 \\ 0 & 0 & 0 & 0 & 0 & 1 \end{bmatrix} \begin{bmatrix} c_2 & 0 & 0 & 0 & s_2 & 0 \\ 0 & c_3 & 0 & 0 & 0 & s_3 \\ 0 & 0 & 1 & 0 & 0 & 0 \\ 0 & 0 & 0 & 1 & 0 & 0 \\ -s_2 & 0 & 0 & 0 & c_2 & 0 \\ 0 & -s_3 & 0 & 0 & 0 & c_3 \end{bmatrix} \begin{bmatrix} 1 & 0 & 0 & 0 & 0 & 0 \\ 0 & 1 & 0 & 0 & 0 & 0 \\ 0 & 0 & c_5 & 0 & s_5 & 0 \\ 0 & 0 & 0 & c_6 & 0 & s_6 \\ 0 & 0 & -s_5 & 0 & c_5 & 0 \\ 0 & 0 & 0 & -s_6 & 0 & c_6 \end{bmatrix}. \quad (2.10)$$

The six angles are defined by the diagonalization condition: $\mathcal{M}_{diag} = \mathcal{N}^T \mathcal{M} \mathcal{N}$, where the diagonalized mass matrix \mathcal{M}_{diag} takes the diagonal form of 2×2 sub-matrices which have non-vanishing symmetric off-diagonal components of the Dirac mass eigenvalues denoted by m_χ , $m_{\psi_{H_1}}$, and $m_{\psi_{H_2}}$.

The sizes of the mixing angles play an important role in determining the cosmic antiproton flux and the direct detection rate as we will discuss in detail in later sections. It is now instructive to find their approximate expression in the limit of small mixing angles: $s_i \ll 1$. In the leading order of $m_Z s_W \ll M_1 < \mu_{1,2}$, the four mixing angles are given by

$$\begin{aligned} s_1 &\approx \frac{c_1 m_Z s_W c_\beta (M_1 + \xi_1 \mu_1)}{M_1^2 - \mu_1^2}, & s_2 &\approx -\frac{c_1 c_2 m_Z s_W s_\beta (c_4^2 M_1 + \xi_2 \mu_2)}{c_1^2 c_4^2 M_1^2 - \mu_2^2}, \\ s_3 &\approx -\frac{c_3 c_4 m_Z s_W s_\beta (c_1^2 \xi_2 M_1 + \mu_2)}{c_1^2 c_4^2 M_1^2 - \mu_2^2}, & s_4 &\approx \frac{c_4 m_Z s_W c_\beta (\xi_1 M_1 + \mu_1)}{M_1^2 - \mu_1^2}, \end{aligned} \quad (2.11)$$

and correspondingly the approximate mass eigenvalues are

$$\begin{aligned} m_\chi &\approx (c_1 c_2 M_1 + s_1 c_2 m_Z s_W c_\beta - s_2 m_Z s_W s_\beta) c_3 c_4 \\ &\quad - (c_1 c_2 \xi_2 m_Z s_W s_\beta - s_2 \mu_2) s_3 + (c_1 c_2 \xi_1 m_Z s_W c_\beta + s_1 c_2 \mu_1) c_3 s_4, \\ m_{\psi_{H_1}} &\approx (s_1 M_1 - c_1 m_Z s_W c_\beta) s_4 + (-s_1 \xi_1 m_Z s_W c_\beta + c_1 \mu_1) c_4, \\ m_{\psi_{H_2}} &\approx (s_3 c_4 M_1 + c_3 \xi_2 m_Z s_W s_\beta) c_1 s_2 + (s_3 c_4 m_Z s_W s_\beta + c_3 \mu_2) c_2. \end{aligned} \quad (2.12)$$

Also in the limit of small s_i and $\xi_i = 1$, the remaining two mixing angles have the form of

$$s_5 \approx s_6 \approx \frac{m_Z^2 s_W^2 s_\beta}{\mu_1 - \mu_2} \left(\frac{c_\beta}{\mu_1} + \frac{1}{\mu_2} \right). \quad (2.13)$$

After the diagonalization, one can find the following interaction vertices of the dark matter particle χ relevant for our analysis:

$$\begin{aligned} \mathcal{L}_f &= \sqrt{2}g'Y_{f_R}\mathcal{N}_{22}[\bar{f}P_L\chi\tilde{f}_R + \bar{\chi}P_Rf\tilde{f}_R^*] \\ &+ \sqrt{2}g'Y_{f_L}\mathcal{N}_{22}[\bar{f}P_R\chi^c\tilde{f}_L + \bar{\chi}^cP_Lf\tilde{f}_L^*], \end{aligned} \quad (2.14)$$

$$\begin{aligned} \mathcal{L}_{h^0} &= \frac{g'}{2}h^0[C_1(\bar{\psi}_{H_1}P_R\chi^c + \bar{\chi}^cP_L\psi_{H_1}) \\ &+ C_2(\bar{\psi}_{H_2}P_R\chi^c + \bar{\chi}^cP_L\psi_{H_2}) \\ &+ C'_1(\bar{\psi}_{H_1}P_L\chi^c + \bar{\chi}^cP_R\psi_{H_1}) \\ &+ C'_2(\bar{\psi}_{H_2}P_L\chi^c + \bar{\chi}^cP_R\psi_{H_2}) \\ &+ 2\delta_S\bar{\chi}\chi], \end{aligned} \quad (2.15)$$

$$\begin{aligned} \mathcal{L}_Z &= \frac{g}{2c_W}Z_\mu[\delta'_1(\bar{\psi}_{H_1}\gamma_\mu P_L\chi^c + \bar{\chi}^c\gamma_\mu P_L\psi_{H_1}) \\ &+ \delta_1(\bar{\psi}_{H_1}\gamma_\mu P_R\chi^c + \bar{\chi}^c\gamma_\mu P_R\psi_{H_1}) \\ &+ \delta'_2(\bar{\psi}_{H_2}\gamma_\mu P_L\chi^c + \bar{\chi}^c\gamma_\mu P_L\psi_{H_2}) \\ &+ \delta_2(\bar{\psi}_{H_2}\gamma_\mu P_R\chi^c + \bar{\chi}^c\gamma_\mu P_R\psi_{H_2}) \\ &+ \delta_V^2\bar{\chi}\gamma_\mu\chi + \delta_A^2\bar{\chi}\gamma_\mu\gamma_5\chi], \end{aligned} \quad (2.16)$$

where

$$\begin{aligned} C_1 &= s_\alpha\mathcal{N}_{22}\mathcal{N}_{33} + c_\alpha\mathcal{N}_{22}\mathcal{N}_{53}, & C_2 &= c_\alpha\mathcal{N}_{22}\mathcal{N}_{55} + s_\alpha\mathcal{N}_{22}\mathcal{N}_{35}, \\ C'_1 &= \xi_1s_\alpha\mathcal{N}_{11}\mathcal{N}_{44} + \xi_2c_\alpha\mathcal{N}_{11}\mathcal{N}_{64}, & C'_2 &= \xi_2c_\alpha\mathcal{N}_{11}\mathcal{N}_{66} + \xi_1s_\alpha\mathcal{N}_{11}\mathcal{N}_{46}, \\ \delta_S &= \frac{1}{2}(s_\alpha\mathcal{N}_{22}\mathcal{N}_{31} + c_\alpha\mathcal{N}_{22}\mathcal{N}_{51} + \xi_1s_\alpha\mathcal{N}_{11}\mathcal{N}_{42} + \xi_2c_\alpha\mathcal{N}_{11}\mathcal{N}_{62}), \\ \delta_1 &= -\mathcal{N}_{44}\mathcal{N}_{42} + \mathcal{N}_{64}\mathcal{N}_{62}, & \delta_2 &= +\mathcal{N}_{66}\mathcal{N}_{62} - \mathcal{N}_{46}\mathcal{N}_{42}, \\ \delta'_1 &= -\mathcal{N}_{33}\mathcal{N}_{31} + \mathcal{N}_{53}\mathcal{N}_{51}, & \delta'_2 &= +\mathcal{N}_{55}\mathcal{N}_{51} - \mathcal{N}_{35}\mathcal{N}_{31}, \\ \delta_V^2 &= \frac{1}{2}(\mathcal{N}_{31}^2 - \mathcal{N}_{51}^2 + \mathcal{N}_{42}^2 - \mathcal{N}_{62}^2), \\ \delta_A^2 &= \frac{1}{2}(\mathcal{N}_{31}^2 - \mathcal{N}_{51}^2 - \mathcal{N}_{42}^2 + \mathcal{N}_{62}^2). \end{aligned} \quad (2.17)$$

Here $Y_{f_{L/R}}$ is the $U(1)$ hypercharge of the left/right-handed fermion $f_{L/R}$ and the corresponding sfermion $\tilde{f}_{L/R}$. The angle α is the usual diagonalization angle of the neutral CP even Higgs bosons. In order to simplify the discussion in our analysis, we will decouple all heavy Higgs bosons by assuming $m_A \gg m_Z$, where m_A is the pseudoscalar Higgs boson mass.

3. Indirect and direct signals of Dirac neutralino DM

In the standard Majorana case, the direct annihilation of two neutralinos to two fermions requires a helicity flip in the final states and is vanishing in the limit of massless fermions, $m_f = 0$. As a consequence of this, the annihilation cross section to light fermions is suppressed by a factor of m_f^2/m_χ^2 . On the other hand, when the neutralino is a Dirac particle this suppression is not present, so that the direct annihilation to leptons is largely enhanced and can be the dominant annihilation channel. In this case, the t -channel annihilation to quarks through squark exchange can be suppressed if $m_{\tilde{q}} \gg m_{\tilde{l}}$ [30].

Then, in the presence of a large Higgsino component in the Dirac neutralino composition, annihilations to gauge and Higgs bosons can also lead to significant hadronic final states. Among them, annihilations to quarks through a Higgs particle exchange are suppressed either by a heavy pseudoscalar Higgs boson in the decoupling limit, or by a suppressed s -wave contribution in the non-relativistic limit, an effect which is present also in the Majorana case.

Under these conditions, we analyze the dominant annihilation channels and the direct detection bound of the Dirac neutralino based on the results obtained in the previous section. In Sections 3.1 and 3.2, along with the dominant annihilation of the Dirac neutralino to leptons we will discuss the other relevant annihilation channels to hadronic final states. We will present the neutralino–nucleon cross sections in Section 3.3. The result of this section will be used in Section 4.3 to constrain the Higgsino component of the Dirac neutralino.

3.1 Annihilations to $\tilde{l}\bar{l}$ and hZ

First, let us consider the t -channel annihilation to leptons through slepton exchange which has to be the dominant annihilation channel to explain the observed energetic electron and positron spectrum. In the case of $m_{\tilde{l}_R} \ll m_{\tilde{l}_L}$, we have

$$\langle\sigma v\rangle_{\tilde{l}\bar{l}} \simeq \mathcal{N}_{22}^4 \frac{2\pi\alpha^2}{c_W^4} Y_{l_R}^4 \frac{m_\chi^2}{(m_{\tilde{l}_R}^2 + m_\chi^2)^2}. \quad (3.1)$$

On the other hand, the case of $m_{\tilde{l}_R} \simeq m_{\tilde{l}_L} \simeq m_{\tilde{l}}$ leads to

$$\langle\sigma v\rangle_{\tilde{l}\bar{l}} \simeq \mathcal{N}_{22}^4 \frac{2\pi\alpha^2}{c_W^4} Y_l^4 \frac{m_\chi^2}{(m_{\tilde{l}}^2 + m_\chi^2)^2}, \quad (3.2)$$

where $Y_l^4 \equiv Y_{l_R}^4 + Y_{l_L}^4$. For the three families of the sleptons having same masses, the above expression must be multiplied by a factor of 3.

The Dirac gaugino t -channel annihilation through Higgsino exchange produces a Higgs and a Z bosons, which can significantly contribute to the cosmic antiproton

flux. The annihilation rate for this mode is

$$\langle\sigma v\rangle_{hZ} \simeq \frac{\pi\alpha^2}{8c_W^4 s_W^2} \frac{\sqrt{m_\chi^2 - \bar{m}_Z^2}}{m_\chi^3} \left\{ \left(\frac{m_\chi^2}{m_Z^2} - 1 \right) \left[(y-z)^2 + (y'-z')^2 - \frac{1}{2} \frac{m_Z^2}{m_\chi^2} (z+z')^2 \right] + \frac{3}{2} (y+y')^2 \right\}, \quad (3.3)$$

where

$$y = \sum_i \frac{m_\chi m_{\psi_{H_i}} C_i \delta_i}{m_i^2}, \quad y' = \sum_i \frac{m_\chi m_{\psi_{H_i}} C'_i \delta'_i}{m_i^2}, \quad z = \sum_i \frac{m_\chi^2 C_i \delta_i}{m_i^2}, \quad z' = \sum_i \frac{m_\chi^2 C'_i \delta'_i}{m_i^2},$$

with $m_i^2 \equiv m_{\psi_{H_i}}^2 + m_\chi^2 - \bar{m}_Z^2$, $\bar{m}_Z^2 \equiv (m_Z^2 + m_h^2)/2$. Here $m_h^2 - m_Z^2 \ll m_\chi^2$ is assumed.

In Section 4, we will present numerical results on the limit of $\langle\sigma v\rangle_{hZ}$ coming from cosmic antiproton fluxes. It is, however, useful to see a qualitative behavior of the small mixing limit: $\delta_i, \delta'_i \ll 1$. Taking $\xi_i = 1$ in Eq. (2.11), the cross section (3.3) reduces to a simple approximated form in the zeroth order of m_Z^2 :

$$\langle\sigma v\rangle_{hZ} \approx \frac{\pi\alpha^2}{4c_W^4} \frac{m_\chi^2}{(m_{\tilde{H}}^2 + m_\chi^2)^2} \left(1 - \frac{m_\chi}{m_{\tilde{H}}} \right)^2 \sin^2(\alpha + \beta), \quad (3.4)$$

where $m_{\psi_{H_1}} \simeq m_{\psi_{H_2}} \simeq m_{\tilde{H}}$ and $M_1 \ll |\mu_i|$ is assumed. The ratio between (3.2) and (3.3) becomes

$$\frac{\langle\sigma v\rangle_{hZ}}{\langle\sigma v\rangle_{\bar{l}l}} \approx \frac{1}{8Y_l^4} \frac{(m_l^2 + m_\chi^2)^2}{(m_{\tilde{H}}^2 + m_\chi^2)^2} \left(1 - \frac{m_\chi}{m_{\tilde{H}}} \right)^2 \sin^2(\alpha + \beta). \quad (3.5)$$

Assuming now $m_{\tilde{l}} \simeq m_{\tilde{H}}$ and $Y_l^4 = 51/16$ (three even leptophilic), we have:

$$\frac{\langle\sigma v\rangle_{hZ}}{\langle\sigma v\rangle_{\bar{l}l}} < \frac{2}{51} \left(1 - \frac{m_\chi}{m_{\tilde{H}}} \right)^2 < \frac{2}{51}. \quad (3.6)$$

Comparing the annihilation cross section to charged leptons compatible with the PAMELA positron excess [21] and the upper bound on the annihilation cross section to hZ from the PAMELA antiproton data [27], presented in Fig. 2 of Section 4, we obtain a conservative limit of $\langle\sigma v\rangle_{hZ}/\langle\sigma v\rangle_{\bar{l}l} \lesssim 0.3$ which can be easily satisfied, as shown in Eq. (3.6). In addition, even for only one lepton channel, the condition is also satisfied: $\langle\sigma v\rangle_{hZ}/\langle\sigma v\rangle_{\bar{l}l} < 2/17 < 0.3$.

3.2 Annihilations through Z

In the zero-velocity limit, the following annihilation channels through s -channel exchange of a Z boson have non-vanishing amplitudes. Compared to Eq. (3.3), these rates contain an extra factor $\sim (m_\chi^2/m_{Z,W}^2) \delta^2$ and thus can be important in certain parameter regions.

The annihilation rate for $\chi\bar{\chi} \rightarrow f\bar{f}$ is

$$\langle\sigma v\rangle_{f\bar{f}} \simeq \frac{2\pi\alpha^2}{c_W^4 s_W^4} \frac{\sqrt{m_\chi^2 - m_f^2}}{m_\chi} \left\{ \frac{m_f^2}{m_Z^4} g_A^2 \delta_A^4 + \frac{m_\chi^2}{(4m_\chi^2 - m_Z^2)^2} \left[2(g_V^2 + g_A^2) + \frac{m_f^2}{m_\chi^2} (g_V^2 - 2g_A^2) \right] \delta_V^4 \right\}, \quad (3.7)$$

where $g_V = (T_3 - 2Q_f s_W^2)/2$ and $g_A = -T_3/2$. The annihilation rates for $\chi\bar{\chi} \rightarrow hZ$ and W^+W^- are respectively given by

$$\langle\sigma v\rangle_{hZ} \simeq \frac{\pi\alpha^2}{c_W^4 s_W^4} \frac{\sqrt{m_\chi^2 - \bar{m}_Z^2}}{m_\chi} \left[\frac{m_\chi^2}{m_Z^4} \left(1 - \frac{m_Z^2}{m_\chi^2} \right) \delta_A^4 + \frac{m_\chi^2}{(4m_\chi^2 - m_Z^2)^2} \left(1 + \frac{2m_Z^2}{m_\chi^2} \right) \delta_V^4 \right], \quad (3.8)$$

$$\langle\sigma v\rangle_{WW} \simeq \frac{\pi\alpha^2}{s_W^4} \frac{m_\chi \sqrt{m_\chi^2 - m_W^2}}{(4m_\chi^2 - m_Z^2)^2} \left(4 \frac{m_\chi^4}{m_W^4} + 16 \frac{m_\chi^2}{m_W^2} - 17 - 3 \frac{m_W^2}{m_\chi^2} \right) \delta_V^4. \quad (3.9)$$

Finally, there is also an annihilation channel $\chi\bar{\chi} \rightarrow 2h$. The annihilation rate for this channel is given by

$$\langle\sigma v\rangle_{2h} \simeq \frac{\pi\alpha^2}{4c_W^4 s_W^4} \frac{(m_\chi^2 - m_h^2)^{3/2}}{m_\chi (4m_\chi^2 - m_Z^2)^2} \delta_V^4. \quad (3.10)$$

Among these four channels, the process $\chi\bar{\chi} \rightarrow 2h$ is the smallest one. The hZ channel is larger than the $f\bar{f}$ channel even for the top quark. Thus, the dominant channels are hZ or W^+W^- . The ratio between the two channels is approximately $\delta_A^4 : \delta_V^4/4$. The ratio between the cross sections for annihilations to $\bar{l}l$ and W^+W^- (hZ) depends on two parameters, m_χ and δ_V (δ_A). The upper bound on the ratio between the annihilation rates for $\chi\bar{\chi} \rightarrow \bar{l}l$ and W^+W^- (hZ) is approximately 0.5 (0.3), as can be seen from Fig. 2. Then, comparing (3.9) and (3.8) with (3.2), one finds the limits: $\delta_V \lesssim 0.3 - 0.03$ and $\delta_A \lesssim 0.2 - 0.02$ depending on m_χ in the mass range $200 \text{ GeV} \leq m_\chi \leq 2000 \text{ GeV}$. Note that the upper limit of δ_V is close to the current sensitivity of the direct detection of DM as will be discussed in the following subsection (see Fig. 1). This will be also confirmed by our numerical analysis performed in a more general parameter space.

3.3 Direct detection through Z and h exchange

The vector interaction via t -channel Z boson exchange (2.16) leads to a *spin-independent* neutralino–nucleon cross section. The cross section for the neutralino–nucleon vector interaction is given by

$$\sigma_{\text{vector}}^{\chi-n,p} \simeq \delta_V^4 \frac{\pi\alpha^2}{64s_W^4 c_W^4} \frac{\mu_n^2}{m_Z^4} \left[\frac{Z}{A} (1 - 2s_W^2) - \frac{1}{2} \right]^2, \quad (3.11)$$

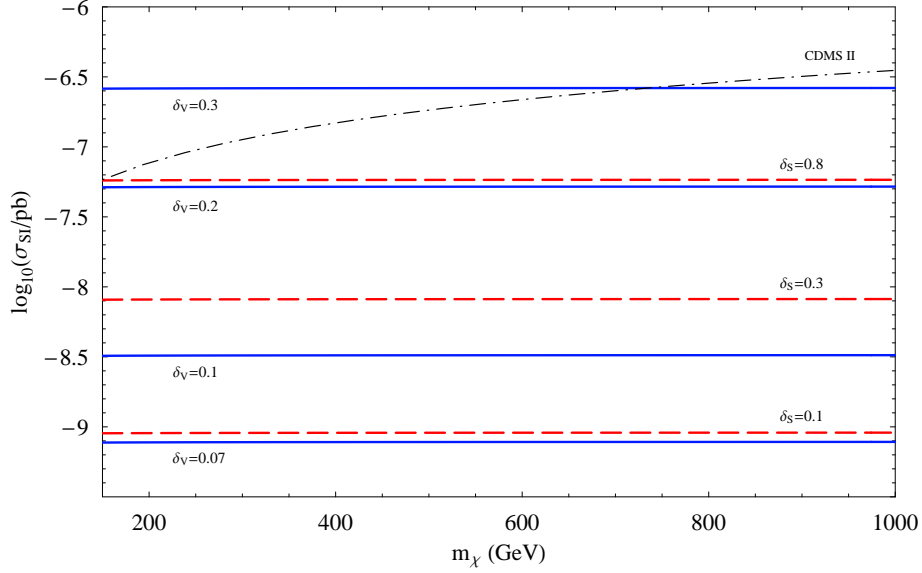


Figure 1: Exclusion plot for the spin-independent neutralino–nucleon cross section σ_{SI} . The (blue) thick solid lines are the cross sections via the vector interaction corresponding to $\delta_V = 0.3, 0.2, 0.1,$ and 0.07 , respectively. The (red) dashed lines are the cross sections through the Higgs exchange corresponding to $\delta_S = 0.8, 0.3,$ and 0.1 , respectively, taking $m_h = 115$ GeV. The dot–dashed line shows the CDMS II limit [26].

where μ_n is the reduced mass for χ -nucleon, and Z and A are the atomic number and the atomic weight of the target nucleus, respectively.

In addition to the vector interaction, the Dirac gaugino χ interacts with nucleons through t -channel Higgs exchange (2.15). The neutralino–nucleon cross section for the scalar interaction is

$$\sigma_{\text{scalar}}^{\chi-n,p} \simeq \delta_S^2 \frac{0.14^2 \times 4g'^2 h_{hss}^2}{\pi} \frac{\mu_n^2 m_n^2}{m_h^4 m_s^2}, \quad (3.12)$$

where h_{hss} is the Higgs–s quark–s quark Yukawa coupling. In the decoupling limit, this result is estimated as

$$\sigma_{\text{scalar}}^{\chi-n,p} \simeq \delta_S^2 \frac{0.14^2 \times 16\pi\alpha^2}{s_W^2 c_W^2} \frac{\mu_n^2 m_n^2}{m_h^4 m_W^2}. \quad (3.13)$$

In Fig. 1, we present the neutralino–nucleon cross sections via the vector interaction (thick solid lines) as a function of m_χ for $\delta_V = 0.3, 0.2, 0.1,$ and 0.07 . The scalar interaction cross sections (dashed lines) are also shown as a function of m_χ for $\delta_S = 0.8, 0.3,$ and 0.1 . The limit from the CDMS II experiment [26] is shown as a dot–dashed line.

4. Analysis

In this section, we analyze the phenomenology of Dirac gauginos in a quantitative way. As discussed in the previous sections, Dirac gauginos can easily meet the requirements of a leptophilic DM candidate, and so we will start in Section 4.1 by summarizing present constraints on generic leptophilic models. We will then proceed in Section 4.2 to discuss specific properties of Dirac binos as leptophilic DM, while in Section 4.3 we will extend the analysis to Dirac neutralinos of generic composition in some particular examples.

4.1 Constraints on leptophilic dark matter

Leptophilic DM annihilation is usually advocated in order to explain simultaneously the PAMELA positron excess [21] and the excellent agreement between the observed antiproton spectrum and the corresponding standard expectation [27]. The present situation of a leptophilic DM candidate annihilating democratically into charged leptons of the three families is summarized in Fig. 2, where the annihilation cross section $\langle\sigma v\rangle$ is plotted as a function of the DM mass m_χ . In particular, the thick and thin closed solid contours show the range of values compatible with the PAMELA positron excess [21] and the FERMI–LAT $e^+ + e^-$ data [25], respectively. The contours are calculated by requiring that the χ^2 per degree of freedom for fits to the data is less than or equal to 1 (only PAMELA data above 10 GeV have been included in the fit), and assuming for the secondary positron and electron backgrounds the conventional GALPROP model denominated by Model #0 in Table 1 of [31]. As far as the propagation model for primary electrons and positrons is concerned, we have adopted a Navarro–Frenk–White (NFW) profile [32] with medium ranges for the diffusion coefficient and for the size of the propagation region, corresponding to the model NFW–med in Table 2 of [33]. The two dot–dashed lines in the upper part of Fig. 2 represent conservative 2 σ C.L. upper bounds for $\langle\sigma v\rangle$ obtained from the flux of $e^+ + e^-$ observed by FERMI [31] (thin line) and the $e^+ + e^-$ flux measured by HESS [24] (thick line).

In the same Figure, we also plot for reference with the short dash–long dash line the upper bound on $\langle\sigma v\rangle$ obtained by considering the imprint on the Cosmic Microwave Background Radiation (CMB) from the injection of charged leptons from DM annihilations at the recombination epoch [34, 35, 36]. In particular, the plotted line is obtained by taking the WMAP5 constraint on the quantity $f\langle\sigma v\rangle$ from Figure 4 of Ref. [34], where f is defined as the average fraction of the DM rest energy deposited in the gas at $z \simeq 800$ –1000, and taking $f \simeq 0.39$ from the analysis of Ref. [35]. As one can see, at present the effect of the CMB constraint on leptophilic models which can explain the PAMELA excess is limited to very large masses, $m_\chi \gtrsim 1.5$ TeV. Future polarization data from Plank will be able to improve this kind of limits considerably [36].

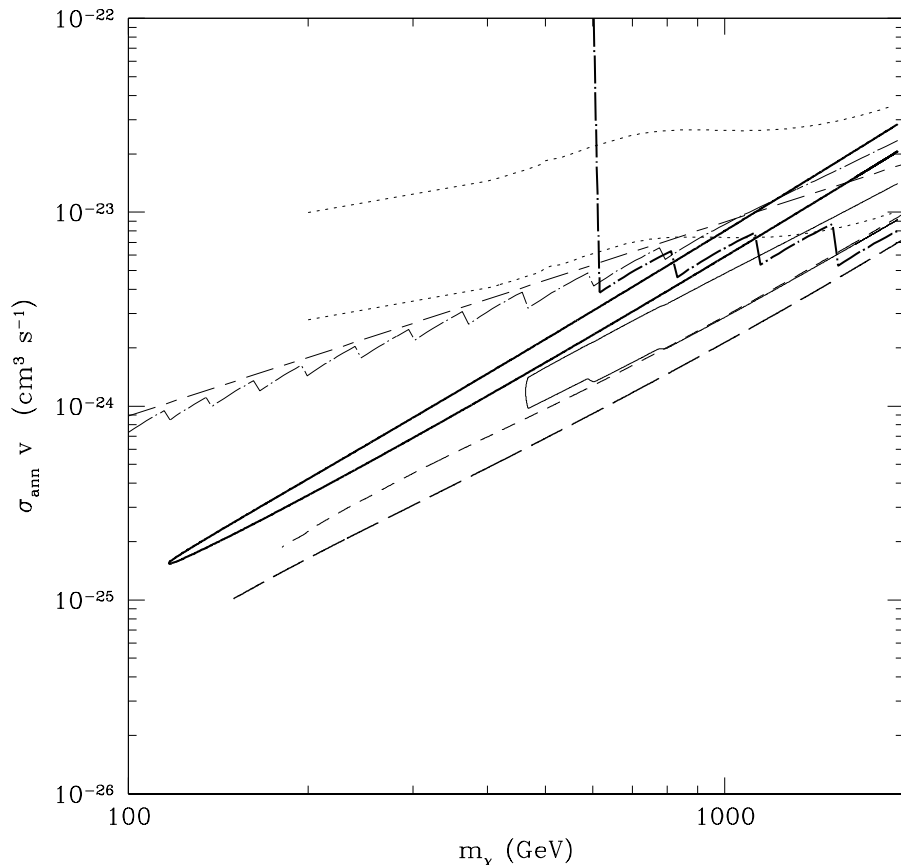


Figure 2: Annihilation cross section times velocity $\langle\sigma v\rangle$ for a DM candidate annihilating democratically to charged leptons of the three families as a function of the mass m_χ . The thick solid contour shows the range of values compatible with the PAMELA positron excess [21]; the thin solid contour is the range compatible to the observed $e^+ + e^-$ flux measured by FERMI-LAT [25]; the thin dot-dashed line is the 2σ upper bound from the observed $e^+ + e^-$ flux of FERMI; the thick dot-dashed line is the 2σ upper bound from the $e^+ + e^-$ HESS measurement [24]; the short dash-long dash line represents the upper bound on $\langle\sigma v\rangle$ from CMB [34, 35, 36]. The lower and upper dotted lines show the upper bound on $\langle\sigma v\rangle$ obtained by comparing the expected gamma-ray flux produced by Inverse Compton (IC) scattering of the final state leptons to the FERMI-LAT measurement of the diffuse gamma ray emission with or without subtraction of the expected standard background, respectively [37]. The short dashed and long dashed lines respectively show the upper bounds on the annihilation cross section to the final states W^+W^- and hZ from the PAMELA antiproton data [27]. See Section 4 for details.

Finally¹, the dotted lines show the upper bounds on $\langle\sigma v\rangle$ obtained by comparing the expected gamma-ray flux produced by Inverse Compton (IC) scattering of the final state leptons to the diffuse flux of gamma-rays measured by FERMI at

¹Signals from DM annihilation in the Galactic Center are very sensitive to the choice of density profile. Therefore, we do not consider them here.

intermediate Galactic latitudes [37]. We do not include in our analysis the preliminary data points very recently released by the FERMI–LAT Collaboration. Due to the large experimental errors, they would not change our conclusions [38]. The upper dotted line has been obtained by directly comparing the flux expected from leptophilic DM (calculated in the approximation of Ref. [39]) to the FERMI–LAT data, while the lower dotted curve has been obtained by subtracting the estimation of the standard background from the data (as a conservative estimation of the latter we have assumed the lower boundary of the dashed region indicated as “Total” in the left–hand panel of Fig. 1 of Ref. [37]).

The IC analysis is described in detail in Fig. 3, where the diffuse FERMI–LAT data at latitudes $10^\circ < b < 20^\circ$ from [37] as a function of the gamma–ray energy E_γ are compared with the corresponding fluxes from leptophilic DM annihilations. In particular, the lower solid curves represent the gamma–ray fluxes from DM annihilation for the representative values $m_\chi=200, 500, 1000, 1500,$ and 2000 GeV (from bottom to top), where for each m_χ the value of $\langle\sigma v\rangle$ is taken from the lower boundary of the thick solid contour of Fig. 2 (that we adopt here and in the following as a conservative estimation for the annihilation cross section required to explain the PAMELA data). The same expected fluxes are also summed to the standard background, shown by the thick solid line in the range $0.1 \text{ GeV} \leq E_\gamma \leq 10 \text{ GeV}$, and the results are plotted in the same energy range. The dashed curves correspond to the predictions for the additional value $m_\chi \simeq 1135$ which, as shown in the magnified inset at the upper–right, can be adopted as an estimation of the upper bound for m_χ from the IC flux.

A comment is in order here. Following other similar analysis in the literature [31, 33], we take the results shown in Fig. 2 as only indicative of the present trends. In fact, it is clear that a consistent χ^2 analysis would require a robust assessment of the systematic uncertainties, an established knowledge of the expected backgrounds² and a full marginalization over the astrophysical parameters, something which is not possible in light of the present uncertainties.

4.2 The Dirac bino as a leptophilic DM candidate

Dirac gauginos can easily meet the requirements of a leptophilic DM candidate, since their annihilation cross section to leptons can be dominant, not being chirality flip suppressed as in the case of Majorana gauginos, while annihilations to quarks potentially capable of producing an excess in the antiproton signal can be inhibited by assuming large masses for the squarks [30]. If the additional hadronic annihilation channels discussed in Sections 3.1 and 3.2 are further suppressed by assuming a negligible Higgsino component in the neutralino composition (by taking $|\mu_{1,2}| \gg M_1$

²At variance with antiprotons, the expected standard background for electrons and positrons could in principle be only in part of secondary origin, with a sizable primary fraction (see for instance [40, 41]).

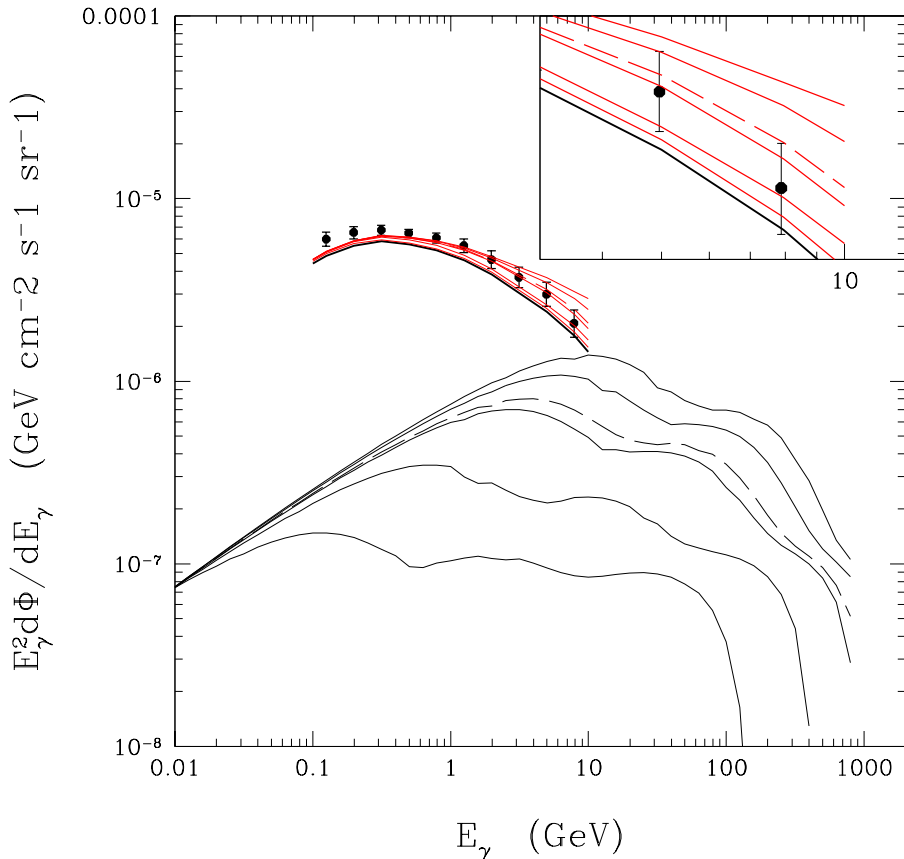


Figure 3: Diffuse gamma-ray flux produced by Inverse Compton scattering of the final state electrons produced in DM annihilations as a function of the gamma-ray energy E_γ for a leptophilic DM candidate annihilating democratically to charged leptons of the three families. The lower solid curves represent the gamma-ray fluxes from DM annihilation for the representative values $m_\chi=200, 500, 1000, 1500,$ and 2000 GeV from bottom to top, where for each m_χ the value of $\langle\sigma v\rangle$ is taken from the lower boundary of the thick solid contour of Fig. 2 (adopted as a conservative estimation for the annihilation cross section required to explain the PAMELA data). The same expected fluxes are also summed to the standard background, shown by the thick solid line in the range $0.1 \text{ GeV} \leq E_\gamma \leq 10 \text{ GeV}$, and the results are plotted in the same energy range. The dashed curves correspond to the IC predictions for the additional value $m_\chi \simeq 1135$ which, as shown in the magnified inset at the upper-right, can be adopted as an estimation of the upper bound for m_χ from the IC flux from our analysis. The experimental points are the FERMI-LAT data at latitudes $10^\circ < b < 20^\circ$ from [37].

in the mass matrix of Eq. (2.9)), a totally leptophilic model is obtained for which only the constraint $m_\chi \lesssim 1 \text{ TeV}$ from the IC flux discussed in Fig. 3 is applied³. The phenomenology of such a DM candidate is quite simple, and is summarized in

³Notice that the IC gamma-ray flux retains the directional information of the source, allowing in principle to establish whether the e^\pm PAMELA excess is diffused in all the Galactic halo or localized,

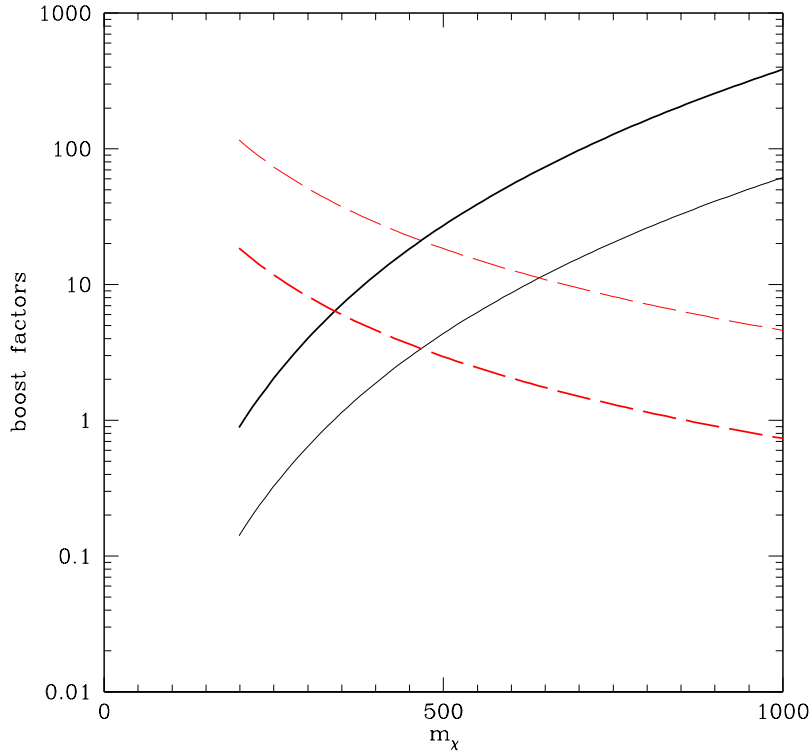


Figure 4: Boost factors for a Dirac gaugino DM candidate annihilating democratically to leptons of the three families as a function of the mass and in the limit $|\mu| \gg M_1$. Solid lines show the ratio between the annihilation cross section required to explain the PAMELA excess and the value of $\langle\sigma v\rangle$ calculated using Eq. (3.2). Dashed lines show the ratio between the observed lower value of the DM relic density $\Omega_{min}h^2 = 0.098$ [42] and the corresponding thermal relic abundance for the Dirac gaugino. Thin lines refer to $m_{\tilde{l}}/m_\chi = 1$ (where we have assumed a small mass splitting between $m_{\tilde{l}}$ and m_χ sufficient to avoid coannihilations between sleptons and neutralinos) while thick ones to $m_{\tilde{l}}/m_\chi = 2$, where $m_{\tilde{l}}$ is the slepton mass.

Fig. 4, where the solid lines show the ratio between the annihilation cross section $\langle\sigma v\rangle$ required to explain the PAMELA data (taken as before from the lower boundary of the thick closed solid contour in Fig. 2) and that calculated by making use of Eq. (3.2) for $m_{\tilde{l}}/m_\chi = 1$ (thin line) and 2 (thick one). In particular, $m_{\tilde{l}}/m_\chi \gtrsim 1$ maximizes the expected annihilation cross section by assuming the lightest possible slepton mass compatible with the requirement that the neutralino is the Lightest Supersymmetric Particle (LSP). In this latter case, the Dirac gaugino annihilation cross section to leptons can explain the PAMELA data for $m_\chi \simeq 330$ GeV, while $m_\chi \simeq 200$ GeV is needed if $m_{\tilde{l}}/m_\chi = 2$.

It is well known, however, that the values of the annihilation cross section that

for instance, in a DM clump close to the Solar System. The preliminary data of Ref. [37] do not provide this piece of information since they are averaged over all galactic longitudes $0^\circ \leq l \leq 180^\circ$.

can explain the PAMELA excess ($\langle\sigma v\rangle \simeq 10^{-24} \text{ cm}^3 \text{ s}^{-1}$) are about two orders of magnitude larger than the range compatible to a standard thermal relic abundance in agreement with observation ($2\text{--}3\times 10^{-26} \text{ cm}^3 \text{ s}^{-1}$ at the decoupling temperature $T \simeq m_\chi/20$). This is naively shown in Fig. 4, where the dashed lines represent the ratio between the 2σ lower value of the observed DM relic density $\Omega_{min}h^2 = 0.098$ [42] and the corresponding thermal relic abundance for the Dirac gaugino. The thin dashed line refers to $m_{\tilde{l}}/m_\chi = 1$ while the thick one to $m_{\tilde{l}}/m_\chi = 2$. From this figure, one can see that a light Dirac gaugino ($m_\chi \lesssim 500 \text{ GeV}$) can explain the PAMELA data with moderate or no boost factor at all if, for instance, some non-standard expansion history of the Universe [43] or non-thermal production mechanism is advocated in order to reconcile its DM relic abundance to the observation. Alternatively, a thermal relic density in agreement with observation is attained for $m_\chi \gtrsim 800 \text{ GeV}$, but in this case a large enhancement of the annihilation cross section to leptons is necessary. Such an enhancement could be provided by an astrophysical boost factor due to substructures, although recent analysis seems to disfavor values larger than order 10 [44]. Furthermore, this piece of information can be combined to the data on $e^+ + e^-$ from FERMI-LAT, which, as shown by the thin closed contour plot in Fig. 2, imply a lower bound on the neutralino mass $m_\chi \gtrsim 465 \text{ GeV}$. Notice, however, that lower values for the mass of the annihilating DM particle can be in principle assumed if some additional contribution to the electron+positron background is claimed at energies $E \gtrsim 1 \text{ TeV}$ to explain the FERMI-LAT data independently [40, 41, 45].

4.3 The case of a Dirac neutralino of general composition

As discussed in Section 3.3, an important phenomenological feature of a Dirac neutralino is the presence of a vector coupling with the Z boson, which on the other hand is vanishing in the Majorana case. This implies that, while in the standard Majorana scenario a diagram with the Z boson exchange can only contribute to the spin-dependent neutralino–nucleon cross section,⁴ for the Dirac case it can lead to a much more sizeable cross section enhanced by a factor of $\simeq A^2$ (see Eq. (3.11)). However, note that the coupling between a neutralino and a Z boson vanishes (as long as the coupling to the Higgs bosons) in the limit $|\mu_{1,2}| \gg M_1$ of a pure gaugino. This implies that the detection of Dirac neutralinos through direct searches is possible only in the presence of a Higgsino component in a Dirac neutralino of arbitrary composition. In order to explore this possibility, we discuss in this section the full parameter space of our model, by allowing $|\mu_{1,2}| \simeq M_1$, and discuss the constraints coming from the hadronic annihilation channels discussed in Sections 3.1 and 3.2. In particular, in Figs. 5 and 6, the $M_1 - \mu_i$ parameter space of the Dirac neutralino is explored for the two representative cases $\mu_1/\mu_2 = 1$ and $\mu_1/\mu_2 = 0.1$. Our numerical analysis is performed in the case of $\xi_1 = \xi_2 = 1$. In each figure, the left-hand

⁴The most stringent limits on pure WIMP–proton and WIMP–neutron spin-dependent cross sections are given by KIMS [46] and ZEPLIN-III [47], respectively.

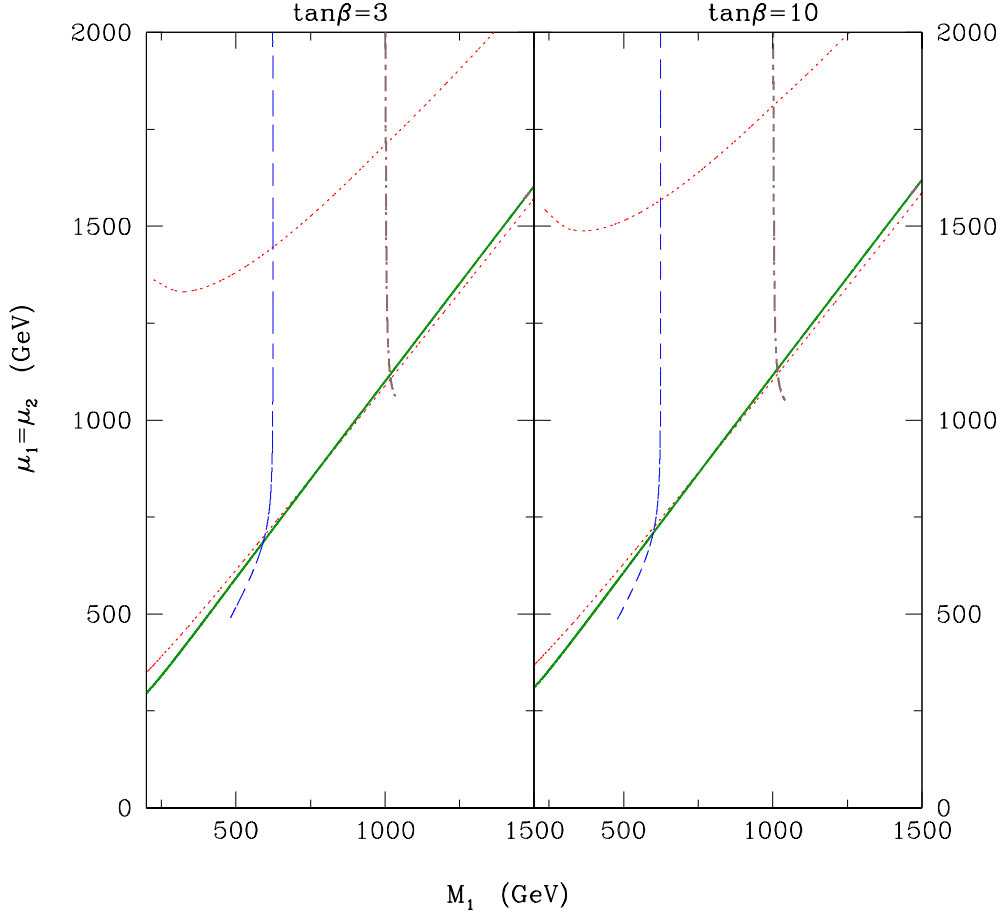


Figure 5: Parameter space for a Dirac neutralino of general composition, for $\mu_1=\mu_2$ and $\tan\beta=3,10$ (left and right panels, respectively). In each panel, the region below the slanted solid line is excluded by the PAMELA antiproton data, while along the two dotted lines the ratio between the neutralino–nucleon scattering cross section calculated with Eqs. [(3.11), (3.12)] and the experimental limit from CDMS II [26] is fixed to 1 (lower curve) and 10^{-3} (upper curve). The regions below the lower dotted curves, where this ratio is larger than 1, are excluded by the direct detection constraint. Moreover, in each plane, the vertical thin dashed line to the left represents points where the boost factor, defined as the ratio between the annihilation cross section $\langle\sigma v\rangle$ required to explain the PAMELA excess and that calculated by making use of Eq. (3.2), is equal to 10, while the vertical thick dot–dashed line to the right represents points at constant mass $m_\chi=1$ TeV.

panel corresponds to $\tan\beta = 3$ and the right–hand panel to $\tan\beta = 10$. In all the $M_1\text{--}\mu_i$ planes, the predominantly Higgsino region below the slanted solid line is excluded by an antiproton flux above the PAMELA data of Ref. [27], driven by the cross section to W^+W^- of Eq. (3.9) and a subdominant contribution from the hZ final state of Eq. (3.3) (in the calculation of the latter cross section we have assumed a supersymmetric Higgs sector in the decoupling limit, $m_{H,A} \gg m_h$, with $m_h=115$ GeV). The corresponding upper bounds to these two cross sections, which as already

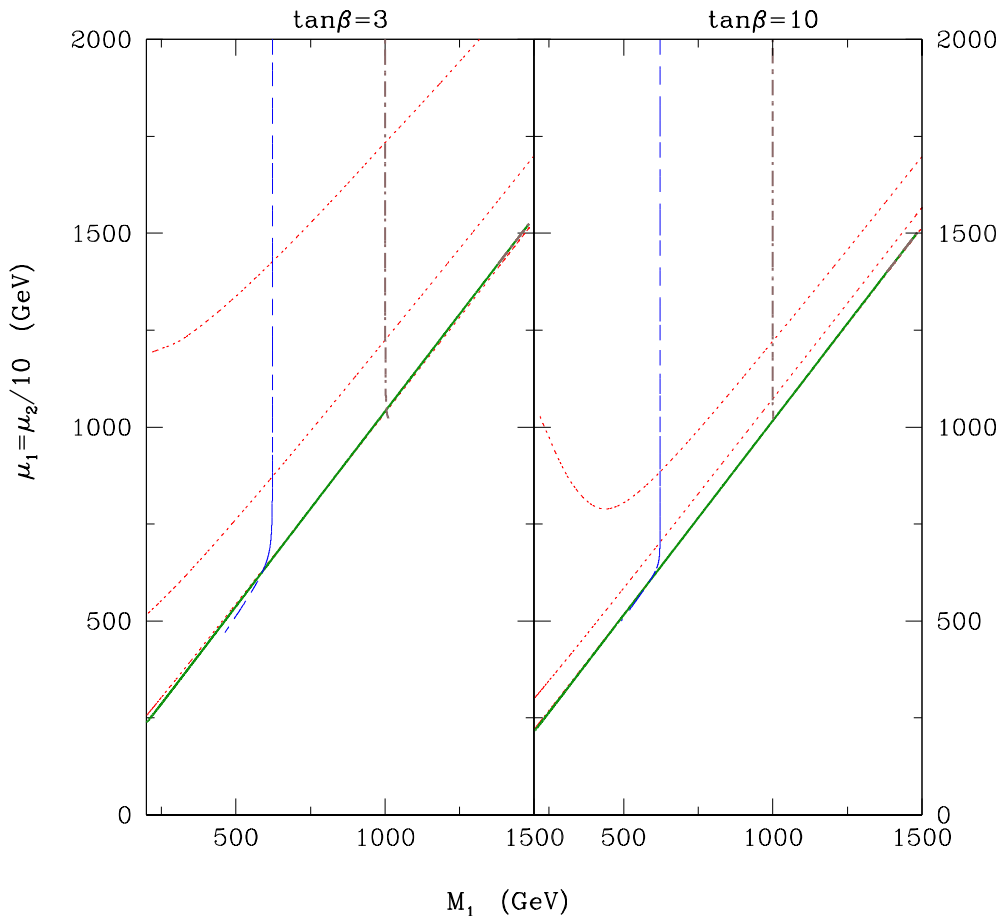


Figure 6: The same as in Fig. 5, with $\mu_2/\mu_1=10$. In both panels, the three dotted lines show points where the ratio between the neutralino–nucleon scattering cross section calculated with Eqs. [(3.11), (3.12)] and the experimental limit from CDMS II [26] is fixed to 1 (lower curve, barely visible in the right–hand panel), 10^{-3} (middle curve), and 10^{-5} (upper curve).

mentioned in Sections 3.1 and 3.2 turn out to be the dominant hadronic ones in our R–symmetric scenario, are plotted for reference in Fig. 2 as short–dashed and long–dashed lines, respectively. They have been obtained by conservatively requiring $\chi^2 < 40$ when comparing the theoretical expectation to the PAMELA data (this value corresponds approximately to a 99.5 % C.L. for 17 degrees of freedom). For the calculation of the antiproton fluxes, we have adopted the NFW–med model for propagation [33] and the parametrization of Ref. [48] for the secondary antiproton background.

In Figs. 5 and 6, the vertical thin dashed line to the left represents points where the boost factor, defined as the ratio between the annihilation cross section $\langle\sigma v\rangle$ required to explain the PAMELA excess and that calculated by making use of Eq. (3.2), is equal to 10. In particular, the points to the right of this vertical line require a larger value. Note that an astrophysical enhancement to the effective cross section provided

by DM substructure larger than order 10 appears to be unlikely [44]. Moreover, in each M_1 - μ_i plane, the vertical thick dot-dashed line to the right represents points with a constant Dirac neutralino mass $m_\chi=1$ TeV. Configurations to the right of this line have larger masses and appear to be disfavored by the IC flux shown in Fig. 3. Note that this is the only irreducible astrophysical bound which is constraining also in the pure gaugino limit $|\mu_i| \gg M_1$.

In the regions of Figs. 5 and 6 that are excluded by antiproton fluxes (below the slanted solid lines), a sizeable Higgsino fraction can also drive the neutralino-nucleon cross section above the present experimental limit. This is shown by the dotted lines which represent configurations with a fixed ratio between the expected neutralino-nucleus cross section and the present experimental upper bound from CDMS II [26]. In particular, in all the $\mu_i - M_1$ planes this ratio is equal to 1, 10^{-3} , and 10^{-5} (if present), starting from the lower curve. In the regions below the lower dotted curves, this ratio is larger than one, so that they are excluded by the present limit from CDMS II.

The expected fluxes for positrons, electrons, and antiprotons, as well as the expected direct detection cross section for a Dirac neutralino are shown in detail in Fig. 7 for the specific example $m_\chi \simeq 465$ and $\langle\sigma v\rangle \simeq 1.4 \times 10^{-24} \text{ cm}^{-3} \text{ s}^{-1}$. This configuration corresponds to the lower mass bound implied by the FERMI-LAT $e^+ + e^-$ data if no additional sources of electrons and positrons are assumed and, as shown in Fig. 4, implies a boost factor of around 3 in the case of $m_{\tilde{\tau}}/m_\chi \simeq 1$ and in the limit of a pure bino. In particular, in Figs. 7a and 7b, the corresponding positron and $e^+ + e^-$ fluxes are plotted as a function of the energy, while the antiproton flux and the neutralino-nucleon cross section are plotted in Figs. 7c and 7d, respectively, for the case of a Dirac neutralino of general gaugino-Higgsino composition in the representative case of $\tan\beta = 3$ and $\mu_1/\mu_2=1$. Note that in the case of a non-negligible Higgsino-gaugino mixing the boost factor for the leptonic annihilation cross section required to explain the PAMELA data, which is plotted in Fig. 4 in the pure gaugino limit $|\mu_i| \gg M_1$, can be somewhat larger due to the suppression of the bino coefficient \mathcal{N}_{22} . However, this effect is not sizeable. For instance, for the maximal Higgsino composition compatible to the CDMS II limit shown by a star in Fig. 7d the boost factor turns out to be $\simeq 4$ instead of $\simeq 3$.

5. Conclusions

Determining the Majorana/Dirac nature of gauginos will be an interesting task for future experiments to look for supersymmetry. Moreover, as an interesting variance of the standard Majorana case, Dirac gauginos can be natural realizations of leptophilic DM, which has been recently proposed to explain the rising positron flux observed in cosmic rays by PAMELA without producing excesses in the antiproton signal. In this paper, we have analyzed the phenomenology of Dirac gauginos in

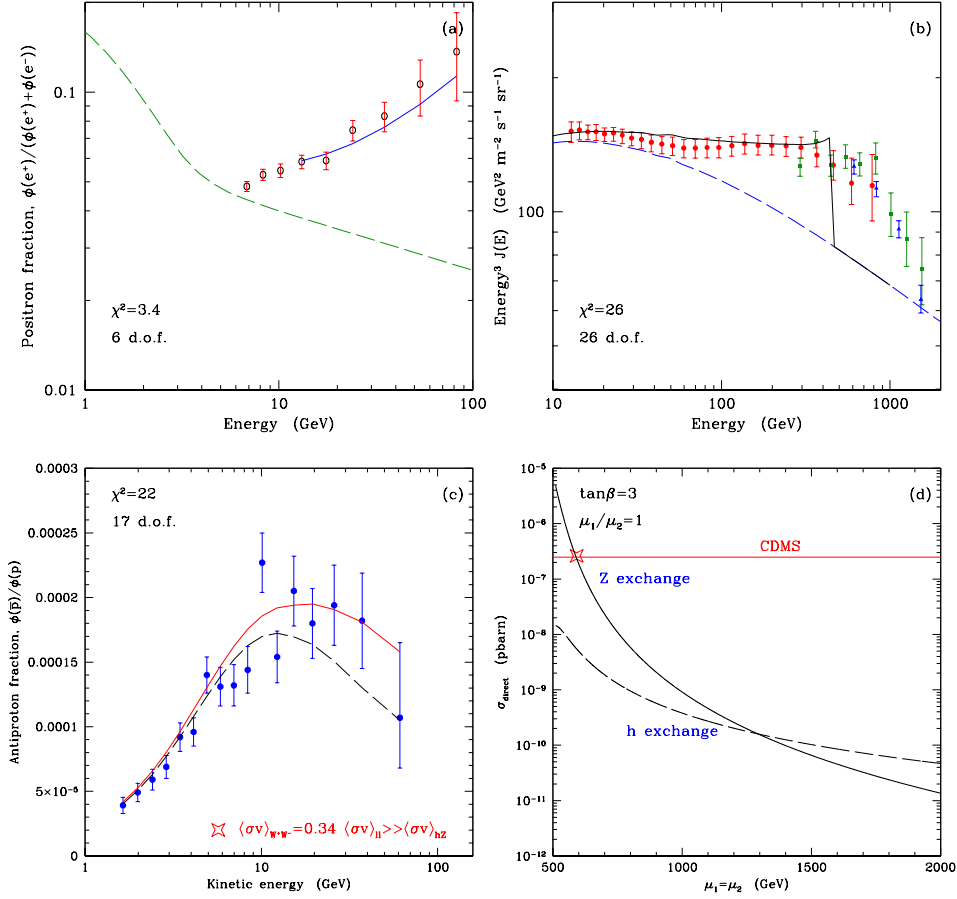


Figure 7: Various observables calculated for the representative configuration $m_\chi = 465$ GeV and $\langle\sigma v\rangle_{\bar{l}l} = 1.4 \times 10^{-24} \text{ cm}^3 \text{ s}^{-1}$. (a) Solid line: positron fraction compared to the PAMELA data [21]. Dashes: secondary background (Model #0 of Ref. [31]); (b) Solid line: electron+positron flux compared to the FERMI–LAT data [31]. Dashes: secondary background (Model #0 of Ref. [31]); (c) Solid line: antiproton fraction compared to the PAMELA data [27]. Dashes: secondary background [48]. The value of the hadronic annihilation cross section $\langle\sigma v\rangle_{W+W^-}$ used for the calculation corresponds to the configuration indicated with a star in panel (d) which is at the level of the experimental CDMS II exclusion plot; (d) Neutralino–nucleon cross section as a function of $\mu_1 = \mu_2$ for $\tan\beta = 3$. The horizontal line is the corresponding CDMS II upper bound [26].

a specific supersymmetric realization, where a continuous R symmetry is assumed to protect vanishingly small Majorana masses. We have shown that a light Dirac gaugino ($m_\chi \lesssim 500$ GeV) can explain the PAMELA data with moderate or no boost factor for light ($\gtrsim m_\chi$) slepton masses. Furthermore, in the case of a non-vanishing Higgsino fraction, Dirac gauginos can have a vector coupling with the Z gauge boson leading to a sizable spin-independent scattering off nuclei. In some specific examples, we have shown that present constraints on the Higgsino fraction of Dirac gauginos

from direct detection experiments are at the same level of those coming from antiproton data. This implies that a Dirac gaugino signal is potentially at the level of the sensitivity of direct detection experiments at present and in the near future.

Acknowledgement: E.J.C. was supported by Korea Neutrino Research Center through National Research Foundation of Korea Grant (2009-0083526). S.S. was supported by the WCU program (R32-2008-000-10155-0) of National Research Foundation of Korea.

References

- [1] L. J. Hall and L. Randall, Nucl. Phys. B **352**, 289 (1991).
- [2] L. Randall and N. Rius, Phys. Lett. B **286**, 299 (1992).
- [3] P. J. Fox, A. E. Nelson and N. Weiner, JHEP **0208**, 035 (2002) [arXiv:hep-ph/0206096].
- [4] A. E. Nelson, N. Rius, V. Sanz and M. Unsal, JHEP **0208**, 039 (2002) [arXiv:hep-ph/0206102].
- [5] Z. Chacko, P. J. Fox and H. Murayama, Nucl. Phys. B **706**, 53 (2005) [arXiv:hep-ph/0406142].
- [6] I. Antoniadis, A. Delgado, K. Benakli, M. Quiros and M. Tuckmantel, Phys. Lett. B **634**, 302 (2006) [arXiv:hep-ph/0507192].
- [7] I. Antoniadis, K. Benakli, A. Delgado and M. Quiros, Adv. Stud. Theor. Phys. **2**, 645 (2008) [arXiv:hep-ph/0610265].
- [8] K. Benakli and C. Moura in M. M. Nojiri *et al.*, arXiv:0802.3672 [hep-ph].
- [9] S. D. L. Amigo, A. E. Blechman, P. J. Fox and E. Poppitz, JHEP **0901**, 018 (2009) [arXiv:0809.1112 [hep-ph]]; M. Luo and S. Zheng, JHEP **0901**, 004 (2009) [arXiv:0812.4600 [hep-ph]].
- [10] L. Alvarez-Gaume and S. F. Hassan, Fortsch. Phys. **45**, 159 (1997) [arXiv:hep-th/9701069].
- [11] J. Hisano, M. Nagai, T. Naganawa and M. Senami, Phys. Lett. B **644**, 256 (2007) [arXiv:hep-ph/0610383].
- [12] G. D. Kribs, E. Poppitz and N. Weiner, Phys. Rev. D **78**, 055010 (2008) [arXiv:0712.2039 [hep-ph]].
- [13] M. M. Nojiri and M. Takeuchi, Phys. Rev. D **76**, 015009 (2007) [arXiv:hep-ph/0701190].

- [14] S. Y. Choi, M. Drees, A. Freitas and P. M. Zerwas, *Phys. Rev. D* **78**, 095007 (2008) [arXiv:0808.2410 [hep-ph]].
- [15] A. Provenza, M. Quiros and P. Ullio, *JCAP* **0612**, 007 (2006) [arXiv:hep-ph/0609059].
- [16] K. Hsieh, *Phys. Rev. D* **77**, 015004 (2008) [arXiv:0708.3970 [hep-ph]].
- [17] R. Harnik and G. D. Kribs, *Phys. Rev. D* **79**, 095007 (2009) [arXiv:0810.5557 [hep-ph]].
- [18] G. Belanger, K. Benakli, M. Goodsell, C. Moura and A. Pukhov, *JCAP* **0908**, 027 (2009) [arXiv:0905.1043 [hep-ph]].
- [19] S. W. Barwick *et al.* [HEAT Collaboration], *Astrophys. J.* **482**, L191 (1997) [arXiv:astro-ph/9703192]; J. J. Beatty *et al.*, *Phys. Rev. Lett.* **93** (2004) 241102 [arXiv:astro-ph/0412230].
- [20] M. Aguilar *et al.* [AMS-01 Collaboration], *Phys. Lett. B* **646**, 145 (2007) [arXiv:astro-ph/0703154].
- [21] O. Adriani *et al.* [PAMELA Collaboration], *Nature* **458**, 607 (2009) [arXiv:0810.4995 [astro-ph]].
- [22] S. Torii *et al.* [PPB-BETS Collaboration], arXiv:0809.0760 [astro-ph].
- [23] J. Chang *et al.* [ATIC collaboration], *Nature* **456**, 362 (2008).
- [24] F. Aharonian *et al.* [H.E.S.S. Collaboration], *Phys. Rev. Lett.* **101**, 261104 (2008) [arXiv:0811.3894 [astro-ph]]; arXiv:0905.0105 [astro-ph.HE].
- [25] A. A. Abdo *et al.* [The Fermi LAT Collaboration], *Phys. Rev. Lett.* **102**, 181101 (2009) [arXiv:0905.0025 [astro-ph.HE]].
- [26] Z. Ahmed *et al.* [CDMS Collaboration], *Phys. Rev. Lett.* **102**, 011301 (2009) [arXiv:0802.3530 [astro-ph]].
- [27] O. Adriani *et al.* [PAMELA Collaboration], *Phys. Rev. Lett.* **102**, 051101 (2009) [arXiv:0810.4994 [astro-ph]].
- [28] N. Arkani-Hamed, S. Dimopoulos, G. F. Giudice and A. Romanino, *Nucl. Phys. B* **709**, 3 (2005) [arXiv:hep-ph/0409232].
- [29] M. A. Luty, *Phys. Rev. Lett.* **89** (2002) 141801 [arXiv:hep-th/0205077].
- [30] S. C. Park and J. Shu, arXiv:0901.0720 [hep-ph]; C. R. Chen, M. M. Nojiri, S. C. Park, J. Shu and M. Takeuchi, arXiv:0903.1971 [hep-ph]
- [31] D. Grasso *et al.* [FERMI-LAT Collaboration], *Astropart. Phys.* **32**, 140 (2009) [arXiv:0905.0636 [astro-ph.HE]].

- [32] J. F. Navarro, C. S. Frenk and S. D. M. White, *Astrophys. J.* **462**, 563 (1996) [arXiv:astro-ph/9508025]; *Astrophys. J.* **490**, 493 (1997) [arXiv:astro-ph/9611107].
- [33] M. Cirelli, R. Franceschini and A. Strumia, *Nucl. Phys. B* **800**, 204 (2008) [arXiv:0802.3378 [hep-ph]].
- [34] S. Galli, F. Iocco, G. Bertone and A. Melchiorri, *Phys. Rev. D* **80**, 023505 (2009) [arXiv:0905.0003 [astro-ph.CO]].
- [35] T. R. Slatyer, N. Padmanabhan and D. P. Finkbeiner, *Phys. Rev. D* **80**, 043526 (2009) [arXiv:0906.1197 [astro-ph.CO]].
- [36] N. Padmanabhan and D. P. Finkbeiner, *Phys. Rev. D* **72**, 023508 (2005) [arXiv:astro-ph/0503486].
- [37] T. A. Porter for the Fermi Collaboration, arXiv:0907.0294 [astro-ph.HE].
- [38] fermi.gsfc.nasa.gov/science/symposium/2009.
- [39] M. Cirelli and P. Panci, *Nucl. Phys. B* **821**, 399 (2009) [arXiv:0904.3830 [astro-ph.CO]].
- [40] S. Profumo, arXiv:0812.4457 [astro-ph].
- [41] P. Blasi, *Phys. Rev. Lett.* **103**, 051104 (2009) [arXiv:0903.2794 [astro-ph.HE]].
- [42] J. Dunkley *et al.* [WMAP Collaboration], *Astrophys. J. Suppl.* **180**, 306 (2009) [arXiv:0803.0586 [astro-ph]].
- [43] P. Salati, *Phys. Lett. B* **571**, 121 (2003) [arXiv:astro-ph/0207396]; F. Rosati, *Phys. Lett. B* **570**, 5 (2003) [arXiv:hep-ph/0302159]; S. Profumo and P. Ullio, *JCAP* **0311**, 006 (2003) [arXiv:hep-ph/0309220]; C. Pallis, *JCAP* **0510**, 015 (2005) [arXiv:hep-ph/0503080]; G. Barenboim and J. D. Lykken, *JHEP* **0612**, 005 (2006) [arXiv:hep-ph/0608265]; D. J. H. Chung, L. L. Everett, K. Kong and K. T. Matchev, *JHEP* **0710**, 016 (2007) [arXiv:0706.2375 [hep-ph]].
- [44] J. Lavalley, J. Pochon, P. Salati and R. Taillet, arXiv:astro-ph/0603796; J. Lavalley, Q. Yuan, D. Maurin and X. J. Bi, arXiv:0709.3634 [astro-ph].
- [45] G. Kane, R. Lu and S. Watson, *Phys. Lett. B* **681**, 151 (2009) [arXiv:0906.4765 [astro-ph.HE]]; L. Zhang, K.S. Cheng, *Astron. Astrophys.* **368** **1063** (2001).
- [46] H. S. Lee. *et al.* [KIMS Collaboration], *Phys. Rev. Lett.* **99**, 091301 (2007) [arXiv:0704.0423 [astro-ph]].
- [47] V. N. Lebedenko *et al.* [ZEPLIN-III Collaboration], *Phys. Rev. Lett.* **103**, 151302 (2009) [arXiv:0901.4348 [hep-ex]].
- [48] F. Donato, D. Maurin, P. Brun, T. Delahaye and P. Salati, *Phys. Rev. Lett.* **102**, 071301 (2009) [arXiv:0810.5292 [astro-ph]].